PHYSICAL ABRASION OF MAFIC MINERALS AND BASALT GRAINS: APPLICATION TO MARTIAN AEOLIAN DEPOSITS

Carin Cornwall

A Thesis
Submitted in Partial Fulfillment of the
Requirements for the Degree of

Master of Science

UNIVERSITY OF WASHINGTON
2014

Committee:
Joshua L. Bandfield
Timothy N. Titus
Charlotte Schreiber
David Montgomery

Program Authorized to Offer Degree:

Earth and Space Sciences

University of Washington

Abstract

PHYSICAL ABRASION OF MAFIC MINERALS AND BASALT GRAINS: APPLICATION TO MARTIAN AEOLIAN DEPOSITS

Carin Cornwall

Chair of the Supervisory Committee:
Dr. Joshua L. Bandfield
Earth and Space Sciences

Sediment maturity, or the mineralogical and physical characterization of sediment deposits, has been used to locate of sediment source, transport medium and distance, weathering processes, and paleoenvironments on Earth. Mature terrestrial sands are dominated by quartz, which is abundant in source lithologies on Earth and is physically and chemically stable under a wide range of conditions while immature sands, such as those rich in feldspars or mafic minerals, are composed of grains that are easily physically weathered and highly susceptible to chemical weathering. On Mars, which is predominately mafic in composition, terrestrial standards of sediment maturity are not applicable. In addition, the martian climate today is cold, dry and sediments are likely to be heavily influenced by physical weathering instead of chemical weathering. Due to differences in weathering processes and composition, martian sediments require an alternate maturity index. Abrasion tests have been conducted on a variety of mafic materials and results suggest that mature martian sediments may be composed of very well sorted, well-rounded, spherical basalt grains with some volcanic glass and chemically altered products. A modified

sediment maturity index is proposed that can be used in future studies to constrain sediment source, paleoclimate, mechanisms for sediment production, and surface evolution. This maturity index may also provide details about erosional and sediment transport systems and preservation processes of layered deposits.

This is dedicated to my parents, Mark and Linda Cornwall, who have supported me through thick and thin, had an unwavering belief in my abilities, and always saw the light at the end of the tunnel.

ACKNOWLEDGEMENTS

I would like to thank Dave McDougall for help involving equipment training and sample preparation in the laboratory, Charlotte Schreiber for her insightful comments and invaluable discussions, Hanson Fong for SEM sample preparation and training, and Mike Harrell for donating some mineral samples and for the use of his modified Bond air mill which made this study possible. This research was partially funded by a University of Washington departmental research grant in the department of Earth and Space Sciences.

Table of Contents

	Page
1. INTRODUCTION	**1**
2. DATA AND SAMPLES	**2**
2.1 Sediment Samples	**2**
2.2 Shape analysis	**3**
2.3 Remote Sensing Data	**4**
3. ANALYSIS TECHNIQUES	**5**
3.1 Analogs	**5**
3.2 Abrasion Tests	**6**
3.3 Shape Analysis	**7**
3.4 Grain Surface Textures	**8**
3.5 Remote Sensing	**9**
4. RESULTS	**11**
4.1 Abrasion and Shape Analysis	**11**
4.2 Grain Texture	**13**
4.3 Thermal Inertia	**14**
5. DISCUSSION	**15**
5.1 Abrasion and Sample Analysis	**15**
5.2 Weathering Textures	**18**
5.3 Thermal Inertia Case Studies	**19**
6. CONCLUSION	**20**
7. REFERENCES	**22**
FIGURES	**25**

1. Introduction

Mineralogical and physical characterization of sediment grains on Earth has been an important area of study that has significantly increased understanding of sediment source, transport medium and distance, weathering processes, and paleoenvironments (e.g., Bagnold, 1941; Folk, 1951, 1954; Suttner and Dutta, 1986; Weltje and Eynatten, 2004; Garcia et al., 2004). The term 'sediment maturity' has been commonly applied to clastic deposits on Earth and describes composition as well as grain texture (Folk, 1951; Boggs, 2006). Sediment maturity refers to the degree in which sediment has been modified by physical and chemical processes. In general, "mature" sediment grains are those that are well rounded, well sorted (consisting of similar sizes), and composed of minerals that are resistant to aqueous and physical weathering (Folk, 1951; Pettijohn, 1975). The majority of mature terrestrial sands are dominated by quartz, which is abundant in source lithologies on Earth and is physically and chemically stable under a wide range of conditions.

On Mars, however, terrestrial standards of sediment maturity are not applicable due to the martian surface having a predominantly mafic composition (e.g., Bandfield, 2002). The presence of mafic minerals indicates sediment immaturity under terrestrial conditions because many mafic minerals are highly susceptible to chemical weathering, are softer than quartz, and contain cleavage planes, making them less durable during physical transport. The martian climate today is cold, dry and dominated by wind-blown (aeolian) activity. Significant aqueous activity on the martian surface is thought to have ended early in the planet's history with geologic evidence relating to liquid water on the surface dating

to over 3 billion years ago (Carr and Head, 2010). Thus, modern sediments are likely to have been largely shaped by physical weathering related to aeolian processes.

Martian sediments require an alternate maturity index that takes into account the absence of significant chemical weathering and the presence of a primary mafic surface composition (Grotzinger et al., 2011; Titus et al., 2012; Fenton et al., 2013). A modified sediment maturity index can be used to place constraints on sediment source, paleoclimate, mechanisms for sediment production, and surface evolution. This maturity index can also provide details about erosional and depositional landscapes (sediment transport systems) and preservation processes of layered deposits. This study explores the physical durability of a variety of geologic materials and investigates the changes in grain texture during a series of abrasion tests. The results of these experiments lead to the construction of a maturity index more appropriate for the martian environment and climate.

2. Data and Samples

2.1 Sediment Samples

The Earth analog samples that I used for this study are mafic sands collected from South Point Beach, Hawaii; Hilo, Hawaii; and the Moses Lake dune field in Washington. The Hawaiian sediments are predominantly composed of olivine (South Point) and volcanic glass (Hilo; Moberly et al., 1965; Marsaglia, 1993). The Moses Lake sediment is composed of granodiorite and basalt grains with minor smectite alteration products (Bandfield et al., 2002). Terrestrial sediment samples were collected and chosen for analysis based on the composition and environment in which they were weathered and deposited. The Hawaiian beach sand samples

originate from a humid, where aqueous activity dominates. The Moses Lake dune field sand originates from a relatively arid environment and was weathered from local volcanic deposits and subsequently transported by aeolian processes. For the purposes of this study, only weathering textures of basaltic grains were analyzed from the Moses Lake sediments. Grains of basalt were manually separated from the granodiorite particles under a microscope.

The abrasion samples were used to determine physical durability of common materials on Mars as well as to provide a comparison to terrestrial quartz-rich sediments. The variety of mafic minerals and volcanic materials were chosen based on remote sensing observations of Mars. The surface of Mars is predominantly basaltic in composition and comprised of minerals rich in magnesium and calcium (e.g., Bandfield, 2002). Therefore, the materials chosen for this study include olivine (forsterite), clinopyroxene (augite), plagioclase (labradorite), volcanic glass and fine-grained basalt from the Columbia River Basalt Group volcanic deposits. The varieties of silica-rich samples that were used to relate abrasion results to familiar terrestrial materials include crystalline quartz, polycrystalline quartz, and microcrystalline chert. Unaltered and compositionally pure mineral samples were ordered from the suppliers Ward's Science (www.wardsci.com) and D.J. Minerals Inc. (www.djminerals.com). Columbia River Basalt Group rock outcrop samples were collected from localities near Moses Lake, Washington.

2.2 Shape Analysis

Measurements of grain size and shape characteristics were made using a CAMSIZER by Retsch Technology. CAMSIZER employs dynamic digital image

processing described in the International Organization for Standardization ISO 13322-2 (www.iso.org). Measurements involve the projection of grain silhouettes in transmitted light as they free fall past the detector from a feeding chute. A high-resolution and low-resolution camera record the projected shadows, allowing for high accuracy size measurements of particles ranging from 30 μm to 30 mm in diameter (e.g. Lo Castro and Andronico, 2009; Guo et al., 2011; Jerolmack et al., 2011). The particle shadows are scanned in 64 directions, providing a precise and detailed analysis of a wide range of particle shapes using CAMSIZER analysis software (e.g., Lo Castro et al., 2009; Miller and Henderson, 2010; Patchigolla and Wilkinson, 2010; Jerolmack et al., 2011). Particle shape parameters that are collected in this study include size, roundness, and sphericity (http://www.retsch-technology.com).

2.3 Remote Sensing Data

Thermal infrared imaging data from Mars Odyssey Thermal Emission Imaging System (THEMIS) was used to examine the thermophysical properties of martian equatorial dune fields (between 50° N and S).

THEMIS infrared images are collected in roughly 1-um-wide bands at nine discrete wavelengths (from ~6.8 to 15 microns) using a 320 by 240 element microbolometer array with a sampling of 100 meters/pixel. The results of three of these equatorial martian dune fields are used as case studies to apply laboratory results presented in this paper to remote sensing observations. The locations of the dune fields were chosen based on their proximity to a potential sediment source. Intercrater dune fields, such as the Schroeter Crater dune field (57.0°E, -2.1°N), accumulate

sediments that are potentially derived locally from the crater walls (e.g., Fenton, 2005; Schneider, 2006). Craters may also serve as sediment sinks and therefore sediment may also originate from a more regional source (Fenton, 2005). The Meroe Patera dune field (68.5°E, 6.8°N) is located west of Meroe Patera, a volcanic caldera. The Nili Patera dune field is located within Nili Patera and is approximately 70 km north of the Meroe Patera dune field. The Nili Patera dune field has been previously studied and may be very similar to the Meroe Patera dune field. The Nili Patera dunes are actively migrating (Silvestro et al., 2010) and thought to be composed of less mature sand that most likely originated from the caldera (Atwood-Stone and McEwen, 2013). Similarly, the Meroe Patera sediments may also originate from the nearby caldera. Lastly, the Valles Marineris dune field located at (282.1°E, -8.9°N) contours the canyon wall and is 5 km south of a large landslide deposit. It is composed of segregated light and dark sediment with distinctly different thermophysical properties and the potential for different source materials and sediment maturity. Each of these case studies provides an opportunity to apply laboratory results to remote sensing observations and explore sediment source, transport and weathering history in different environments on Mars.

3. Analysis Techniques.

3.1 Analogs

SEM images were used to investigate differences in grain weathering textures between humid (Hawaiian) and arid (Moses Lake) climates and to determine the amount of influence aqueous processes have on shaping volcanic sediments (Marshall et al., 1987). In addition, to better constrain the effects of

aqueous weathering, the basaltic grains from Moses Lake were also compared to the abraded Columbia River basalt sample to investigate differences in grain texture and to see if the physical weathering textures present on the Moses Lake basalt grains could be replicated using a Bond air mill.

3.2 Abrasion Tests

In preparation for abrasion, the mafic minerals, silica-rich materials, and Columbia River basalt were crushed, sifted and sorted into approximate equidimensional grain shapes with sizes between 2 – 3 mm. Abrasion tests were conducted using a modified Bond air mill following the design and convention of Nitkiewicz and Sterner (1988). The modified Bond air mill used in this study has similar dimensions to the mill employed by Nitkiewicz and Sterner (1988, Fig. 1) and is composed of 320 μm silicon carbide grit mixed with epoxy resin, with copper tubing for the air entrance. Compressed air is connected to the air entrance of the mill through rubber tubing and, when turned on, causes mineral fragments within the chamber to rapidly roll around the interior cylindrical track and quickly become well rounded and spherical.

Each abrasion experiment consisted of 100 grains, following the grain analysis method of Rosenfeld et al. (1953), and was conducted for each mineral and volcanic material separately. These samples are hereafter referred to as the homogenous samples. The final abrasion experiment consisted of a mixture of 50% basalt grains and remaining 50% equal parts mafic minerals and materials including: olivine, pyroxene, labradorite, volcanic glass, and a Mg-rich phyllosilicate. A basaltic mixture was included in the abrasion tests to simulate martian surface

conditions in an aeolian environment and to ultimately investigate potential differences in abrasion rates and durability of minerals abraded together. This sample is hereafter referred to as the heterogeneous sample.

Due to the small size of the Bond air mill, 10 separate batches of 10 grains were run at a time to provide data for 100 grains for each sample composition. To ensure consistency between batches, grains were weighed so that each batch only had a difference of ± 0.005 g, as larger differences tended to cause grains to abrade more rapidly or slowly than other batches, thus introducing inconsistences in abrasion rates. Grains were abraded using a constant flow of compressed air at approximately 20 psi to ensure the grains were not being abraded at a different rate than other batches. The airflow used was strong enough to roll the grains rapidly around the cylindrical track inside the air mill. A fine mesh was glued over the air exit on the mill and prevented grains larger than 400 μm from escaping. The air exit also ensured that significant amounts of dust did not accumulate in the mill resulting in variable abrasion effectiveness between samples.

Each homogenous batch was run at increments of 15 minutes for the first hour then 30-minute increments for another hour and 30 minutes. The homogeneous samples were primarily used to investigate relative rates of changes in grain morphology and size of each separate material. The heterogeneous batches were abraded in increasing time increments until all material was gone and was also used to rank the durability of each material in a basaltic mixture.

3.3 Shape Analysis

The majority of the grain shape analysis was conducted using CAMSIZER dynamic digital image processing software. Shape measurements, including size, roundness, and sphericity, were collected on the terrestrial analog samples and each homogenous grain sample before abrasion and after each abrasion run. Grain size is calculated from the number of pixels a grain silhouette occupies in images captured by the high and low-resolution cameras inside CAMSIZER. Grain roundness is computed using the formula:

$$4\pi A/P^2,$$

where A is the area of the grain silhouette and P is the perimeter of the grain. Roundness values close to 1 indicate that a grain is very well rounded. Sphericity measurements are calculated by dividing the width by length of the grain (minimum extension divided by the maximum extension). Values close to 1 indicate that a grain shape is highly spherical.

In addition, the amount of material being abraded during the abrasion tests was recorded for the homogenous samples. Sediment samples were weighed prior to abrasion and in-between each abrasion run and recorded as the percentage of material lost to equalize between variances in mineral properties and small differences in sample weights.

3.4 Grain Surface Textures

Details of grain surface textures and the effects of chemical and/or physical weathering were examined for the terrestrial analog sediments as well as a few abraded samples using a scanning electron microscope (JEOL – JSM5200). SEM images were taken of the Hawaiian samples, Moses Lake dune field sediment, as

well as the abraded crystalline olivine, volcanic glass and Columbia River Basalt from the homogenous samples. Grains were mounted on a specimen stub using carbon tape and sputter-coated with gold to prevent the accumulation of electrostatic charge on the grain surface during imaging. For the Hawaiian and Moses Lake samples, a series of images were captured at a variety of magnifications to accentuate evidence of chemical and physical weathering on the grain surfaces (Krinsley and Doornkamp, 1973; Margolis and Krinsley, 1974; Marshall et al., 1987). A series of images at various magnifications were also taken for the abraded samples to explore the textures created using the Bond air mill. Comparing grain surface textures of Earth analog and abraded samples provides a way to determine how much of an influence aqueous weathering has on grain morphology and how grain textures might differ from this in the arid martian environment.

3.5 Remote Sensing

THEMIS band nine observations (centered at 12.57 μm) were utilized for brightness temperatures to derive thermophysical properties due to the relatively low spectral response to dust (Smith et al., 2003) and the high signal to noise ratio. Brightness temperatures were derived from calibrated radiance images and corrected for instrumental effects using methods described in Christensen et al. (2004), Bandfield et al. (2004), and Edwards et al. (2011). This study uses nighttime temperatures when thermal contrast due to particle size is at a maximum and to ensure that the effects of albedo and sun-lit slopes have largely dissipated (e.g., Kieffer et al., 1977; Palluconi and Kieffer, 1981; Christensen, 1982). Despite the relatively low spectral response to dust in band 9 observations, large amounts of

suspended atmospheric dust have a significant effect on thermal inertia estimates due to their radiative contributions to surface temperature. IR dust opacities were recorded from THEMIS daytime observations that spatially overlapped and were within ±10° L_s in the same Mars year of the THEMIS nighttime observations that were used to derive thermal inertia maps. To ensure thermal inertia estimates were not significantly affected by atmospheric dust, 9 micron dust opacities were restricted to < 0.2 (Smith et al., 2003). Band 9 observations are significantly affected by the presence of water ice clouds and, therefore, only the observations with the lowest ice opacities were used in this study (< 0.1).

Thermophysical properties were derived from THEMIS data using the KRC thermal model in "one-point" mode (Kieffer, 2013). The KRC model assumes lateral surface homogeneity, Lambertian surface reflection, a surface emissivity of unity, as well as a one-layer spectrally gray atmosphere at solar and infrared wavelengths that is radiatively coupled to the surface and allows for the direct and diffuse insolation using a two-stream delta-Eddington model (Kieffer, 2013). Surface and subsurface temperatures are computed using the heat conduction equation that takes into account a surface boundary condition that includes upward emission and downwelling thermal radiation as well as direct and diffuse illuminations. The "one-point" mode does not take into account effects of CO_2 frost, radiative contributions from adjacent surfaces, the thermal effects of subsurface layers, shadowing of crater or canyon walls, condensate clouds, or the latent heat of water ice (Kieffer, 2013). In addition, thermophysical properties were assumed to be vertically homogenous for this study.

The parameters that were used to derive thermal inertia included THEMIS IR band nine brightness temperatures, central dune field latitude and longitude, visible wavelength dust opacity, time of day, and L_s. Latitude and longitude values are used to extract elevation (atmospheric pressure) and albedo values from the Mars Orbiter Laser Altimeter (Smith et al., 2001) and the Thermal Emission Spectrometer data maps, respectively. IR dust opacities were converted to visible wavelength dust opacities for use in the KRC model by scaling the IR opacities by a factor of 2, according to the visible/9-μm extinction opacity ratio (Clancy et al., 1995; Wolff and Clancy, 2003). By varying thermal inertia values and keeping the input parameters constant, a look up table is created and a temperature is estimated for each thermal inertia value. THEMIS temperatures are compared to values in the look up table and used to interpolate thermal inertia. The thermal inertia maps were imported to a geographical information system and compared to THEMIS daytime infrared surface mosaics (Edwards et al., 2011) for each dune field location included in this study.

4. Results

4.1 Abrasion and Shape Analysis

Grain shape and rounding changed most dramatically within the first 15 minutes of abrasion for all samples. The rate of material loss was also the greatest during the first 15 minutes (Fig. 2) as angular grain edges were chipped off and smoothed. Once grain edges became more smoothed, the rate of material loss significantly decreased and grains became increasingly rounded (Fig. 3). The homogenous sample of olivine obtained the highest degree of sphericity and grain rounding of all the minerals after two hours of abrasion (Fig. 3) and was also the

first mineral sample to be eroded to particles <400μm (Fig. 2). Augite and labradorite were also quickly abraded but became flat and oblong and never achieved high sphericity like the olivine grains (Fig. 3). The most durable materials of the homogenous samples were the volcanic glass and the Columbia River Basalt (Fig. 2). Of the mafic materials, the volcanic glass and basalt were the slowest to decrease in grain size and increase in sphericity and roundness (Fig. 3). After 2 hours and 30 minutes, the volcanic glass and basalt grains had the lowest value of roundness (Fig. 3).

Of the silica-rich materials, polycrystalline quartz was the most durable and mono-crystalline quartz was the least durable. After two hours of abrasion, mono-crystalline quartz grains had a higher sphericity and similar rounding values to polycrystalline quartz and chert (Fig. 4). Chert grains were more durable than crystalline quartz but less durable than polycrystalline quartz and had a higher sphericity compared to polycrystalline quartz after 2 hours of abrasion (Fig. 4). Grain shape characteristics of silica-rich samples were compared to olivine, volcanic glass, and basalt and shape analysis results suggest that the basalt grain morphologies evolve similarly to polycrystalline quartz grains (Fig. 4). Grain shapes for volcanic glass during abrasion evolved differently than the basalt grains and the morphology more closely matched crystalline quartz in regards to sphericity and rounding (Fig. 4). The greatest difference between crystalline quartz and volcanic glass was grain size, where crystalline quartz grains were smaller after 2 hours of abrasion (Fig. 4). Olivine grain shapes evolved much quicker and did not abrade similarly to any kind of silica-rich material.

The abrasion results for the heterogeneous sample are slightly different than that of the homogenous samples. Grain shapes evolved at a slower rate and the materials, especially olivine, lasted longer during abrasion (Fig. 5). The Mg-rich phyllosilicate rapidly broke down into thin sheets and fine-grained particles after the first 15 minutes of abrasion and was eventually abraded into particles <400μm. After 75 minutes of abrasion, the phyllosilicate material was completely gone from the air mill (Fig. 5). After another 120 minutes of abrasion, augite was also abraded to dust while a few larger grains of labradorite persisted for much longer. Olivine grains persisted significantly beyond 2 hours of abrasion, compared to the homogenous abrasion results, and outlasted the labradorite by 60 minutes (Fig. 5). The basalt and volcanic glass grains are the most durable materials but the basalt significantly outlasted the volcanic glass by 3 hours of abrasion (Fig. 5). After 7 hours of abrasion, both the basalt and the volcanic glass grains had achieved high values of rounding and sphericity, comparable to those recorded for the olivine grains in the homogenous sample.

4.2 Grain Texture

SEM images of Hawaiian grain surfaces show more evidence of aqueous weathering textures than the Moses Lake dune field sediments and both samples displayed abundant physical weathering textures. The olivine grains from South Point Beach, Hawaii show extensive chemical pitting on the grain surfaces, (Fig. 6a) as well as scratches (Fig. 6b) and chipping from abrasion. The surface of the Hilo, Hawaii volcanic glass sample is covered in microscopic gas vesicles and displays similar chemical pitting and scratching textures as identified on the olivine grain but

there is more evidence of chipping. Chipping textures were primarily observed inside depressions of gas vesicles (Fig. 6c). The surfaces of the basalt grains from the Moses Lake dune field are not as smooth as the sand grains from Hawaii. Chemical pitting was identified on the basalt grains but scratches and chipping are not as obvious. The basalt grains also display a number of microscopic fractures, typically radiating out from a central point (Fig. 6d). Microscopic fractures are not present on any of the Hawaiian samples that were analyzed.

The abraded homogenous samples of olivine, volcanic glass, and basalt show similarities in grain surface textures due to physical abrasion to that of the Hawaiian and Moses Lake samples. The surface of an un-abraded Columbia River basalt grain is shown in Figure 7a and displays the textural differences between the abraded basalt (Fig. 7b) and the terrestrial analog sample (Fig. 7c). The abraded samples lack evidence of chemical weathering influences and, instead, show extensive signs of chipping and scratching on all grain surfaces (Fig. 7b). These surface textures are far more pervasive on the abraded samples than the terrestrial analog samples. The most notable difference between the sediment samples is the overall smoothness of the grains. The abraded grains are rougher than the terrestrial analog samples, having sharp edges and debris fragments clinging to the surface (Fig. 8b). The only non-aqueous texture that was not observed on the abraded basalt grains is radiating fractures.

4.3 Thermal Inertia

The martian dune fields in this study have significantly different thermophysical properties. The Schroeter Crater dune field is a large sand sheet

with a few barchanoid, transverse and dome dune forms near the perimeter of the dune field and closer to the East-facing crater wall. Of the three dune field locations, the Schroeter Crater dunes have the lowest thermal inertia, ranging from 129 to 211 Thermal Inertia Units (TIU; Fig. 8). The Meroe Patera dune field is comprised of barchans and barchanoid dune forms with thermal inertia values ranging between 186 to 281 TIU (Fig. 9). Finally, the Valles Marineris dune field contours a southern canyon wall and is situated near large landslide deposits on the canyon floor to the north. It is composed of a sand sheet and barchanoid dune forms with two different sediment populations. One sediment population is composed of dark sand with evenly spaced, linear ripples that cover the dune slopes. The second population of sand is composed of lighter sediment with chaotic, discontinuous ripple forms. The darker sediments are superimposed on top of the lighter sediments (Fig. 10). The darker sand has a higher thermal inertia than the lighter sand and ranges between 297-358 TIU. The lighter sand has a thermal inertia between 243 to 278 TIU (Fig. 10).

5. Discussion

5.1 Abrasion and Shape Analysis

The rapid changes in grain size and morphology within the first 15 minutes of abrasion are due to the rounding and chipping of jagged edges and, for some minerals, cleaving along planes of weakness. This process creates multiple small grains and the rate of material lost declines as grains attain a more physically stable, spherical form.

Olivine was the least durable material abraded of the homogenous samples. It has a similar Mohs hardness to quartz with identical fracturing habits but may be more susceptible to abrasion due to differences in crystalline structure and density (Willets, 1983). Minerals that possess cleavage planes, such as labradorite and augite, were moderately durable and abraded into thin, elongate, tabular grains. A comparison between different forms of quartz showed discrepancies in abrasion rates. Crystalline quartz was found to abrade quicker than polycrystalline quartz. Polycrystalline quartz is composed of multiple quartz crystals of variable grain sizes, or, in the case of chert, composed of multiple quartz crystals of equal sizes. Crystalline quartz is "mono" crystalline, meaning it is composed of a single crystal as opposed to multiple crystal grains. Previous studies have shown that mono-crystalline structures are less durable during physical transport than polycrystalline forms due to the formation of micro-fractures that easily propagate through a single crystal (Harrell and Blatt, 1978). The Griffith 'Fracture Theory' describes how pre-existing flaws in a crystalline structure result in macroscopic fractures that spread under stress (Brace, 1961). These fractures also form in polycrystalline materials but fractures do not propagate past individual grain boundaries, resulting in an increased resistance to physical stress (Brace, 1961).

The Columbia River basalt grains were the most durable material tested in this study with grain morphologies that evolved similarly to polycrystalline quartz during abrasion. Basalt is also polycrystalline, being composed of a variety of mafic minerals of variable grain sizes, such as olivine, plagioclase and pyroxene. This

suggests that mechanical durability on Mars may not be controlled by the physical properties of individual minerals but rather by crystalline structure.

The heterogeneous sample abrasion results were used as a basis for a mafic sediment maturity index (Fig. 11). Minerals lasted longer during abrasion most likely due to the addition of the phyllosilicate mineral, which rapidly broke apart into thin sheets and fine particles, resulting in decreased effectiveness of abrasion inside the air mill. The Columbia River basalt grains outlasted the volcanic glass during abrasion but both materials have an extremely high mechanical durability. Martian dune fields composed of mature sediments could be composed of a mixture of basalt and volcanic glass grains as well as chemically derived minerals such as sulfates and salts.

Immature sediments are likely to include pyroxenes and plagioclase in the sediment and the source material is most likely local (Fig. 11). The morphologic differences to that of spherical grains would cause these minerals to be sorted differently during aeolian transport. Some wind tunnel experiments have shown that grains with a lower sphericity were more readily transported than spherical grains but only at low wind speeds (Williams, 1964; Willetts et al., 1982). Particles having a low sphericity also had longer and flatter saltation trajectories than spherical grains but spherical grains exhibited more aeolian bed activity, whereas low sphericity grains were less frequently dislodged (Willetts, 1983; Rice, 1991). Thus, aeolian transport is the most effective for spherical grains. It is likely that minerals with cleavage planes will become segregated from spherical grains and accumulate in different areas of a dune field but it is improbable that these grains

with a low sphericity will be transported long distances. Therefore, it is unlikely that plagioclase and pyroxene minerals will be present in mature aeolian sediments, which have traveled far from the sand source.

The presence of olivine in an aeolian deposit depends on multiple factors including, availability, transport distance, and crystalline structure of the mineral. Source material may be olivine rich or olivine poor basalts, affecting the amount of olivine available for aeolian transport. Olivine also has a higher density than most mafic minerals and volcanic materials, which may result in selective transport of less dense particles especially at low wind speeds (Willetts, 1983). Aeolian sorting effects due to density differences may limit the distance olivine grains travel from the source material. Lastly, mono-crystalline olivine is likely to be less durable during physical transport than polycrystalline olivine. If martian olivine grains are polycrystalline, there should be an enrichment of olivine in aeolian deposits compared to other mafic minerals and the source material.

5.2 Weathering Textures

The Earth analog sediment samples have smoother grain surfaces than the abraded grain samples (Fig. 7). This suggests that even in arid environments, such as Moses Lake, aqueous processes have a considerable impact on grain surface texture. Grains on Mars have probably been predominantly shaped by mechanical weathering with little aqueous interaction and may have rougher surfaces textures similar to those created from the abrasion tests. In addition, immature deposits may be composed of grains that are more angular with rougher surface textures compared to immature terrestrial sediments. Alternatively, martian grains may

have been subject to some aqueous weathering depending on their location and age of the deposit. Aqueous influences would most likely be found in inactive dune fields that have been stabilized by geochemical cements (Gardin et al., 2011) or seasonal ice (Bourke, 2005). Polar aeolian deposits and equatorial aeolian deposits may have significantly different grain textures, with polar sediment grains having smoother surfaces than equatorial grains due to the interaction with seasonal frost deposition and sublimation. Fracturing observed on the surfaces of Moses Lake basalt sands could not be replicated by abrasion alone. The presence of fractures suggests some type of physical process and may be due to cycles of heating and cooling. It is possible that martian basaltic grains also have microscopic fractures on their surfaces.

5.3 Thermal Inertia Case Studies

The Schroeter Crater dune field is one of many intercrater aeolian deposits on Mars. Sediment sources for intercrater dunes could be derived locally from the crater walls or craters could serve as sediment sinks to grains originating from a more regional source. The low thermal inertia of the Schroeter Crater dune field, compared to the other two dune fields in this study suggests a much smaller grain size. This could indicate that the sediment in Schroeter Crater has a regional source, where the sediments have been abraded into smaller grains due to the longer transport distances. If this is the case, the dune field may be composed of entirely basaltic grains with a component of volcanic glass and stable secondary minerals that have been chemically weathered.

The Meroe Patera dune field may be an example of locally derived sediment. These dunes are located west of a volcanic vent and previous studies have suggested that the sediments are less mature due to differences in lee slope angles (angle of repose) to that of other active dunes (Atwood-Stone and McEwen, 2013). If these dune fields are, in fact, composed of immature sediment, they should contain less stable minerals such as pyroxene and plagioclase.

The Valles Marineris dune field in this study contains two distinctly different sediment populations. Thermophysical properties suggest that the light material is finer-grained than the dark material. The dark material also seems to be superimposed on the light material suggesting that the light material is less active (or inactive) than the darker sediments. The finer-grained lighter material could have a more regional source and over time, only the most stable minerals/material remain. The darker material may have a local source, either from the canyon walls or the landslide deposits on the floor of the canyon. Alternatively, this could be an example of aeolian sorting due to differences in grain shape and composition.

6. Conclusion

Abrasion of a variety of mafic materials indicates that super mature sediment compositions may predominantly be composed of very well sorted, well-rounded, spherical basalt grains with some volcanic glass and chemically altered products (Fig. 11). Olivine grains may be present in mature sediments especially if the grains are polycrystalline. Immature sediments are likely to contain minerals with cleavage planes and be poorly sorted, sub rounded and angular (Fig. 11).

SEM images indicate that in arid environments, grain surface textures are still heavily influenced by aqueous interaction. Aqueous weathering produces smoother surfaces than physical weathering alone. Physical weathering processes have dominated the surface of Mars for the past 3 billion years and therefore, grain surfaces are likely to have rougher textures.

The dune fields located in Schroeter Crater (57.0°E, -2.1°N), Meroe Patera (68.5°E, 6.8°N), and Valles Marineris (282.1°E, -8.9°N) have significantly different thermophysical properties. Schroeter Crater dune field is composed of sediment with a low thermal inertia, suggesting it is composed of finer sediment than either the Meroe Patera dune field or the Valles Marineris dune field. This may suggest that the dune material has been transported farther and is composed of more mature sediment. The Meroe Patera dune field has been previously studied and suggested to have a local sediment source (Atwood-Stone and McEwen, 2013). If these sediments are local, the sediments should reflect a less mature composition and larger grain size. The Valles Marineris dune field contains two distinct populations of sediments. The two sediment populations may be derived from two different sediment sources or may reflect aeolian sorting effects due to differences in grain morphology.

7. REFERENCES

Atwood-Stone, C. and A. S. McEwen (2013) Avalanche slope angles in low-gravity environments from active Martian sand dunes, Geo. Phys. Res. Lett., 40, doi:10.1002/grl.50586.

Bagnold, R. A. (1941) The physics of blown sand and desert dunes, Progress in physical geography, 18, 91-96.

Bandfield, J. L. (2002) Global mineral distributions on Mars, J. Geophys. Res., 107, doi:10.1029/2001JE001510.

Bandfield, J. L., K. S. Edgett, and P. R. Christensen (2002) Spectroscopic study of the Moses Lake dune field, Washington: Determination of compositional distributions and source lithologies, JGR, 107, doi:10.1029/2000JE001469.

Bandfield, J. L., D. Rogers, M. D. Smith, and P. R. Christensen (2004) Atmospheric correction and surface spectral unit mapping using Thermal Emission Imaging System data, J. Geophys. Res., 109, doi:1000810.1029/2004JE002289.

Boggs Jr., S. (2006). *Sedimentology and Stratigraphy*. Pearson Education. ISBN 0-13-154728-3.

Bond, W. L. (1951) Making of small spheres, Review of Scientific Instruments, 52, 344-345.

Bourke, M.C (2005) Niveo-aeolian and Denivation Deposits on Mars, Drylands: linking landscape processes to sedimentary environments, BGRG/BSRG International Conference, London.

Brace, W. F. (1961) Dependence of fracture strength of rocks on grain size, 4th Symposium on Rock Mechanics, Penn. State Univ., 99-103.

Carr, M. H. and J. W. Head (2010) Acquisition and history of water on Mars, In Lakes on Mars, Elsevier, 31-67.

Christensen, P. R. (1982) Martian dust mantling and surface composition: Interpretation of thermophysical properties, J. Geophys. Res., 87, 9985-9998.

Christensen, P. R. and 10 colleagues (2004) The Thermal Emission Imaging System (THEMIS) for the Mars 2001 Odyssey Mission, Space Sci. Rev., 110, 85-130.

Clancy, R. T., S. W. Lee, G. R. Gladstone, W. W. McMillan, and T. Rousch (1995) A new model for Mars atmospheric dust based upon analysis of ultraviolet through infrared observations from Mariner 9, Viking, and Phobos, J. Geophys. Res., 100, 5251-5263.

Edwards, C. S., K. J. Nowicki, P. R. Christensen, J. Hill, N. Gorelick, and K. Murray (2011) Mosaicking of global planetary image datasets: 1. Techniques and data processing for Thermal Emission Imaging System (THEMIS) multi-spectral data, J. Geophys. Res., 116, doi:1000810.1029/2010JE003755.

Fenton, L. K. (2005) Potential sand sources for the dune fields in Noachis Terra, Mars, J. Geophys. Res., 110, doi:10.1029/2005JE002436.

Fenton, L. K. et al. (2013) Summary of the Third International Planetary Dunes Workshop: Remote sensing and imaging analysis of planetary dunes, Flagstaff, Arizona, USA, June 12-15, 2012, Aeolian Res. 8, 29-38.

Fergason, R. L., P. R. Christensen, and H. H. Kieffer (2006) High-resolution thermal inertia derived from the Thermal Emission Imaging System (THEMIS): Thermal model and applications, J Geophys. Res., 111, doi:10.1029/2006JE002735.

Folk, R. L. (1951) Stages of textural maturity in sedimentary rocks, J. Sed. Res., 21, 127-130.
Folk, R. L. (1954) The distinction between grain size and mineral composition in sedimentary-rock nomenclature, J. Geology, 62, 344-359.
Garcia, D., C. Ravenne, B. Marechal, and J. Moutte (2004) Geochemical variability induced by entrainment sorting: Quantified signals for provenance analysis, Sed. Geology, 171, 113-128.
Gardin, E., M. C. Bourke, P. Allemand, and C. Quantin (2011) High albedo dune features suggest past dune migration and possible geochemical cementation of aeolian sediments on Mars, Icarus, 212, 590-596.
Grotzinger, J., D. Beaty, G. Dromart, S. Gupta, M. Harris, J. Hurowitz, G. Kocurek, S. McLennan, R. Milliken, G. G. Ori, and D. Sumner (2011) Mars sedimentary geology: Key concepts and outstanding questions, Astrobiology, 11, doi:10.1089/ast.2010.0571.
Guo Zhengyang,Liu Cuilian,Ren Chunhong, and Wang Ying (2011) Comparison of three methods for measuring particle size distribution of polyethylene powder, China Synthetic Resin and Plastics, Beijing Research Institute of Chemical Industry,SINOPEC,Beijing 100013,China.
Harrell, J. and H. Blatt (1978) Polycrystallinity: Effect on the durability of detrital quartz, J. Sed. Pet., 48, 25-30.
Jerolmack, D. J., M. D. Reitz, and R. L. Martin (2011) Sorting out abrasion in a gypsum dune field, J. Geophys. Res., 116, DOI: 10.1029/2010JF001821
Kieffer, H. H., T. Z. Martin, A. R. Peterfreund, B. M. Jakosky, E. D. Miner, and F. D. Palluconi (1977) Thermal and albedo mapping of Mars during the Viking primary mission, J. Geophys. Res., 82, 4249-4291.
Kieffer, H. H. (2013) Thermal model for analysis of Mars infrared mapping, J. Geophys. Res., 118, 451-470.
Krinsley, D. H. and J. C. Doornkamp (1973) “Atlas of Quartz Sand Surface Textures”, Cambridge Univ. Press, London.
Lo Castro M.D. and D. Andronico (2009) Grain size distributions of volcanic particles by CAMSIZER, Conferenza Rittmann, Nicolosi (Ct), Italy, 11-13.
Lo Castro M.D., D. Andronico, G. Nunnari, A. Spata, and A. Torrisi (2009) Shape measurements of volcanic particles by CAMSIZER, Conferenza Rittmann, Nicolosi (Ct), Italy, 11-13.
Margolis, S. V. and D. H. Krinsley (1974) Processes of formation and environmental occurrence of microfeatures on detrital quartz grains, American J. Sci, 274, 449-464.
Marsaglia, K. M. (1993) Basaltic island sand provenance, GSA Special Papers, 284, 41-66.
Marshall, J. R., W. B. Whalley, and D. H. Krinsley (1987) The origin of some “chemical” textures on quartz-grain surfaces: Interpretation and environmental implications, In “Clastic Particles: Scanning Electron Microscopy and Shape Analysis of Sedimentary and Volcanic Clasts” (Marshall, J. R. Ed.), pp. 248-253, Van Nostrand Reinhold, New York.
Miller, N. A. and J. J. Henderson (2010) Quantifying sand particle shape complexity using a dynamic, digital imaging technique, Agronomy J., 102, 1407-1414.

Moberly, R. L., D. Baver, and A. Morrison (1965) Source and variation of Hawaiian littoral sand, J. Sed Res., 35, 589-598.
Nitkiewicz, A. M. and S. M. Sterner (1988) An improved Bond air mill for the preparation of spherical single crystals, American Mineralogist, 73, 662-666.
Palluconi, F. D., and H. H. Kieffer (1981) Thermal inertia mapping of Mars from 60 S to 60 N, Icarus, 45, 415-426.
Patchigolla, K. and D. Wilkinson (2010) Crystal shape characterization of dry samples using microscopic and dynamic image analysis, Particle & Particle Systems Characterization, 26, 171-178.
Pettijohn, F. J. (1975) Sedimentary Rocks, New York: Harper and Row.
Rice, M. A. (1991) Grain shape effects on aeolian sediment transport, Acta Mechanica Supplementum, 1, 159-166.
Rosenfeld, M. A., L. Jacobsen, and J. C. Ferm (1953) A comparison of sieve and thin-section technique for size analysis, J. Geol., 61, 114-132.
Schneider, R. D. (2006) Evidence for locally-derived, ultramafic intracrater materials in Amazonis Planitia, Mars, Masters thesis, University of Hawaii.
Silvestro, S., L. K. Fenton, D. A. Vaz, N. T. Bridges, and G. G. Ori (2010), Ripple migration and dune activity on Mars: Evidence for dynamic wind processes, Geophys. Res. Lett., 37, doi:10.1029/2010GL044743.
Smith et al. (2001) Mars Orbiter Laser Altimeter: Experiment summary after the first year of global mapping of Mars, J. Geophys. Res., 106, 23689-23722.
Smith, M. D., J. L. Bandfield, P. R. Christensen, and M. I. Richardson (2003) Thermal Emission Imaging System (THEMIS) infrared observations of atmospheric dust and water ice cloud optical depth, J. Geophys. Res., 108, doi:511510.1029/2003JE002115.
Suttner, L. J., and P. K. Dutta (1986) Alluvial sandstone composition and paleoclimate, I. Framework mineralogy, J. Sed. Pet., 56, 329-345.
Titus, T. N., R. K. Hayward, and M. C. Bourke (2012) Interdisciplinary research produces results in the understanding of planetary dunes, Eos, Transactions American Geophysical Union, 91 (32), 281.
Weltje, G. J., and H. von Eynatten (2004) Quantitative provenance analysis of sediments: review and outlook, Sed. Geology, 171, 1-11.
Williams, G. (1964) Some aspects of the eolian saltation load, Sedimentology, 3, 257-287.
Willetts, B. B., M. A. Rice, S. E. Swaine (1982) Shape effects in aeolian grain transport, Sedimentology, 29, 409-417.
Willetts, B. B. (1983) Transport by wind of granular materials of different grain shapes and densities, Sedimentology, 30, 669-679.
Wolff, M. J. and R. T. Clancy (2003) Constraints on the size of Martian aerosols from Thermal Emission Spectrometer observations, J. Geophys., Res, 108, doi:509710.1029/2003JE002057.

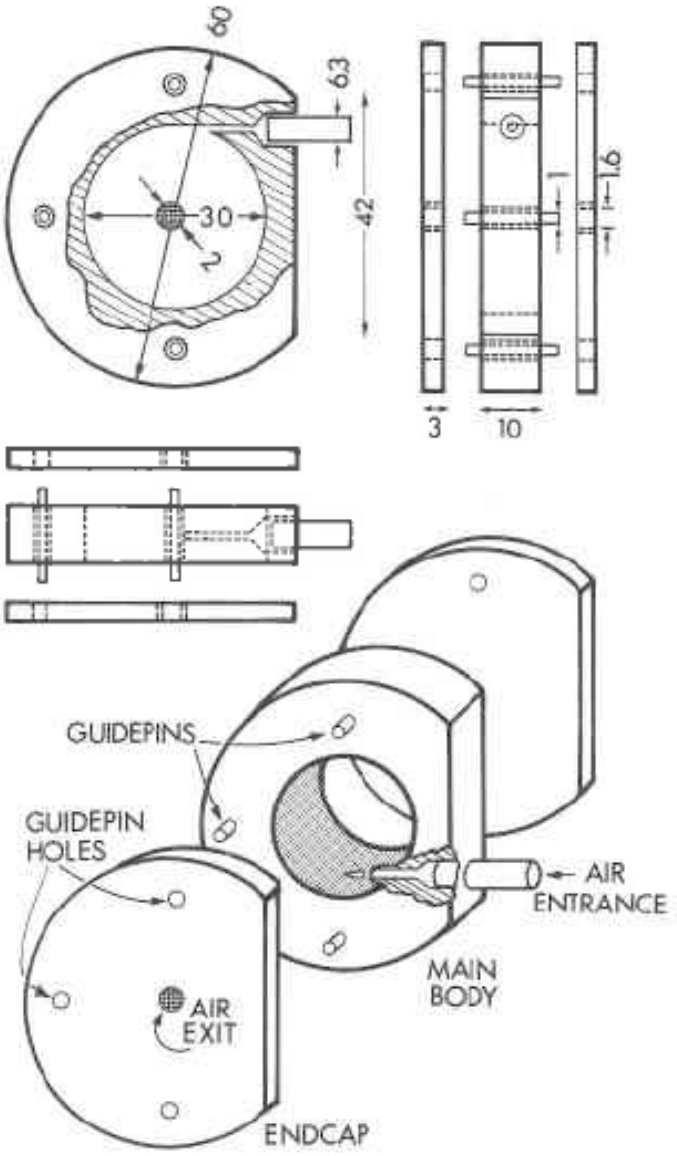

Figure 1. Figure taken from Nitkiewicz and Sterner, 1988 showing design and dimensions (in mm) of Bond air mill. The modified air mill used in this study has similar dimensions and is composed entirely of silicon carbide with copper tubing for the air entrance but lacks guidepins.

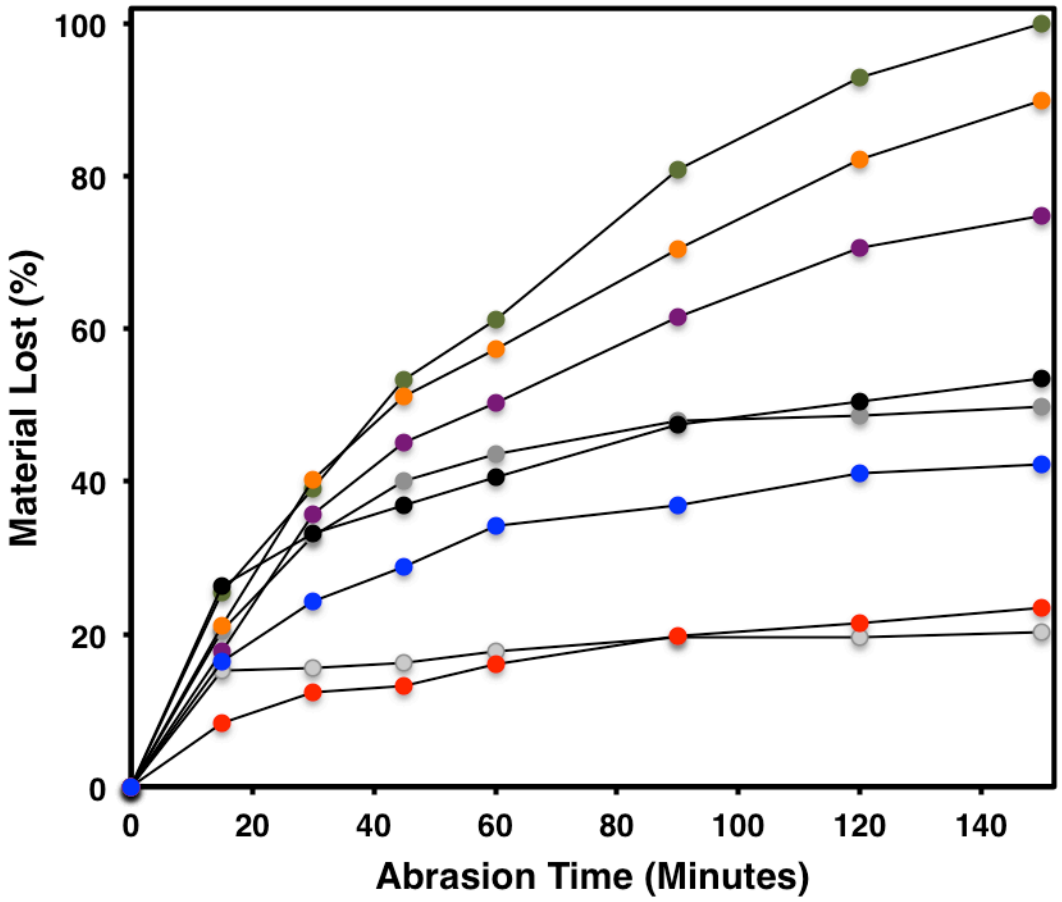

Figure 2. Rate of material loss vs abrasion time in minutes. Colors correspond to Columbia River Basalt, red; polycrystalline quartz, light gray; chert, blue; volcanic glass, black; crystalline quartz, dark gray; labradorite, violet; augite, orange; and olivine, green.

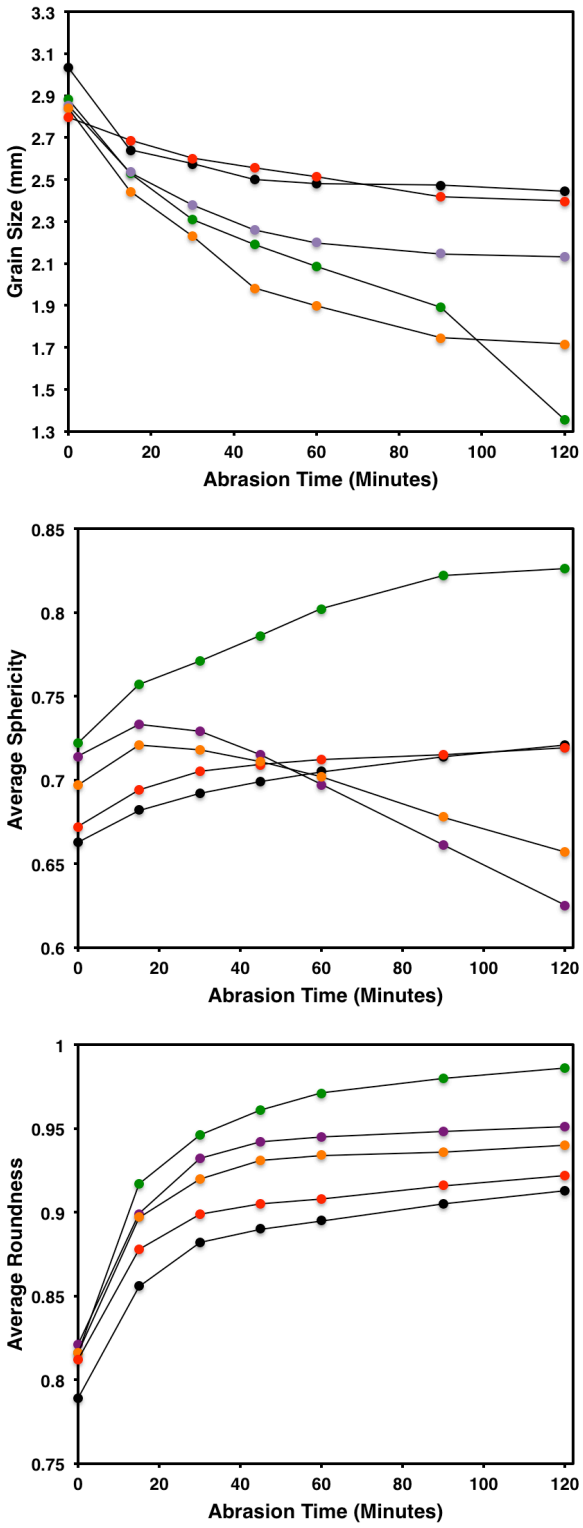

Figure 3. Sphericity vs volume percent of sample for olivine (green), Columbia River Basalt (red), volcanic glass (black), augite (orange), and labradorite (violet) after 2 hours of abrasion. Olivine had the highest sphericity while minerals with cleavage (labradorite and augite) had the lowest sphericites.

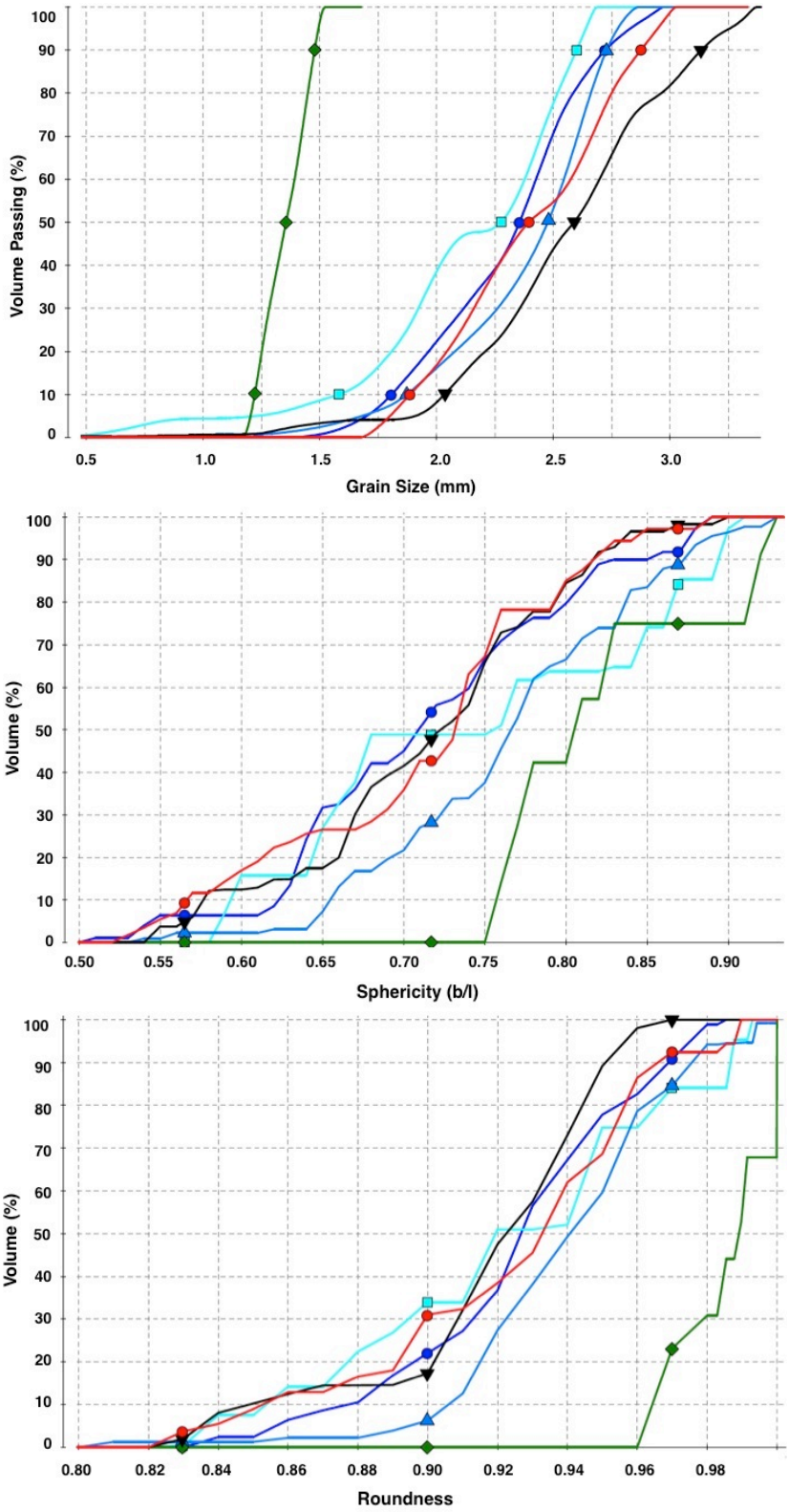

Figure 4. (A) Grain size vs % material passing a particular sieve size, (B) sphericity (b/l) vs sample volume percent, and (C) rounding (SPHT) vs sample volume percent of crystalline quartz (light blue), polycrystalline quartz (dark blue), Columbia River Basalt (red), volcanic glass (black), and olivine (green).

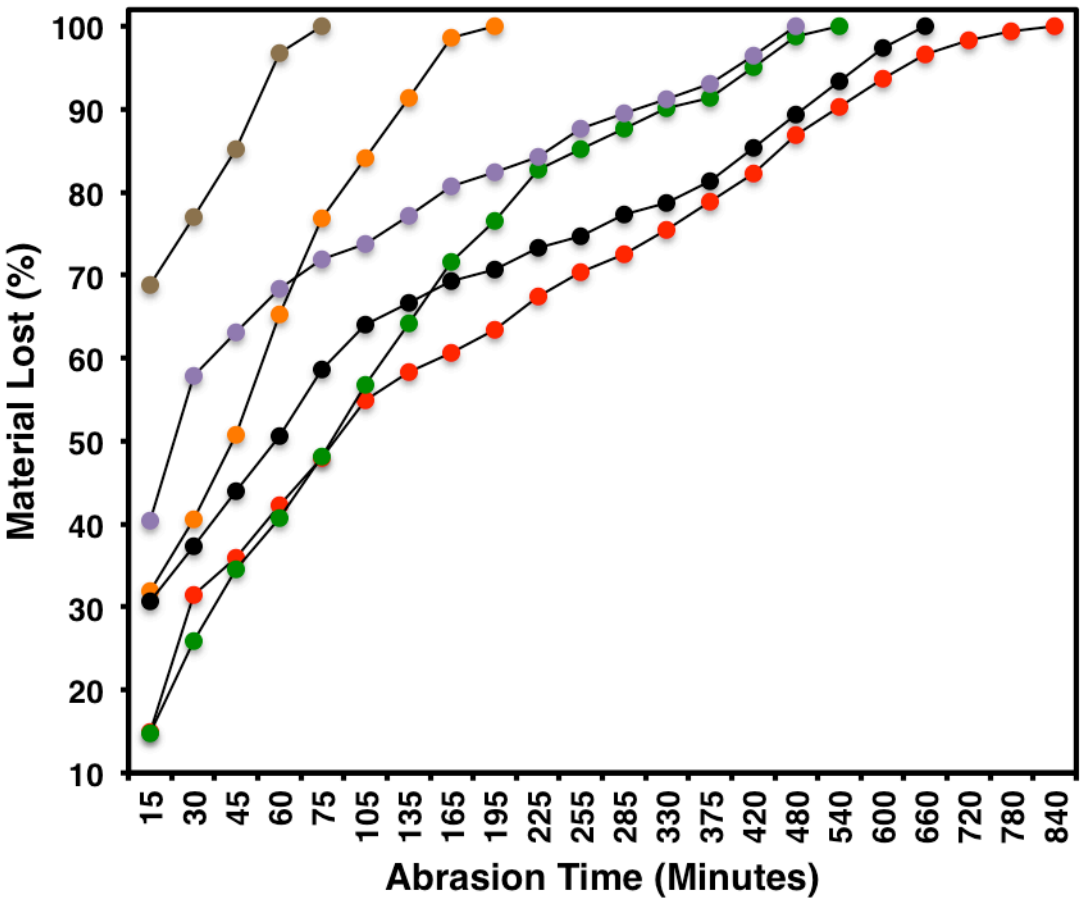

Figure 5. Heterogeneous abrasion results showing percent of material lost vs time in minutes. Heterogenous abrasion sample consisted of 50% Columbia River Basalt (red) and remaining parts equal portions of olivine (green), labradorite (violet), augite (orange), and phyllosilicate (brown).

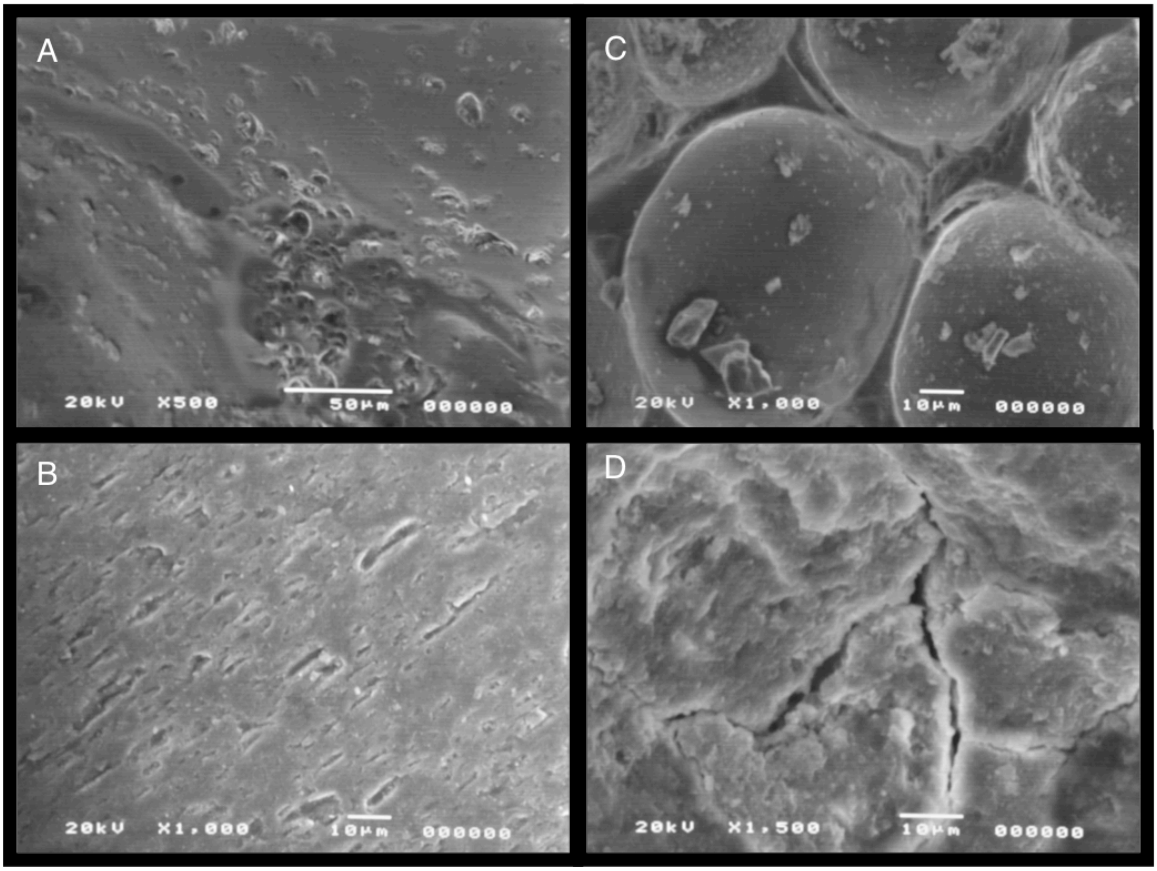

Figure 6. Chemical and physical weathering textures of terrestrial grains (Krinsley and Doornkamp, 1973; Marshall et al., 1987). (A) aqueous pitting due to chemical weathering on an olivine grain from South Point Beach, Hawaii. (B) scratches due to abrasion on the same olivine grain (C) Gas vesicles and chipping on the surface of a volcanic glass grain from Hilo, Hawaii (D) Fracture on the surface of a basalt grain from Moses Lake.

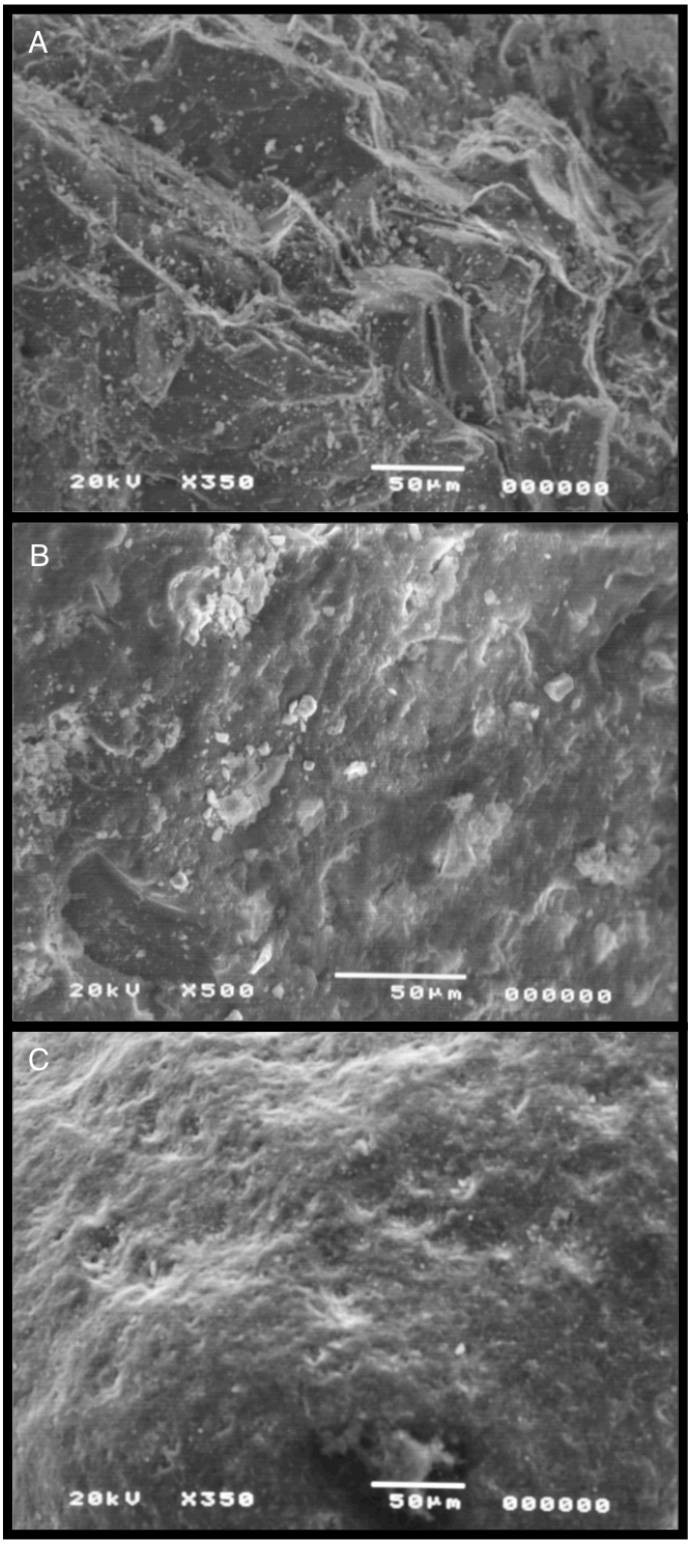

Figure 7. Differences in grain textures of basalt grains. (A) Unabraded Columbia River Basalt grain (B) Abraded Columbia River Basalt after ~14 hours of abrasion and (C) Basalt grain from Moses Lake dune field.

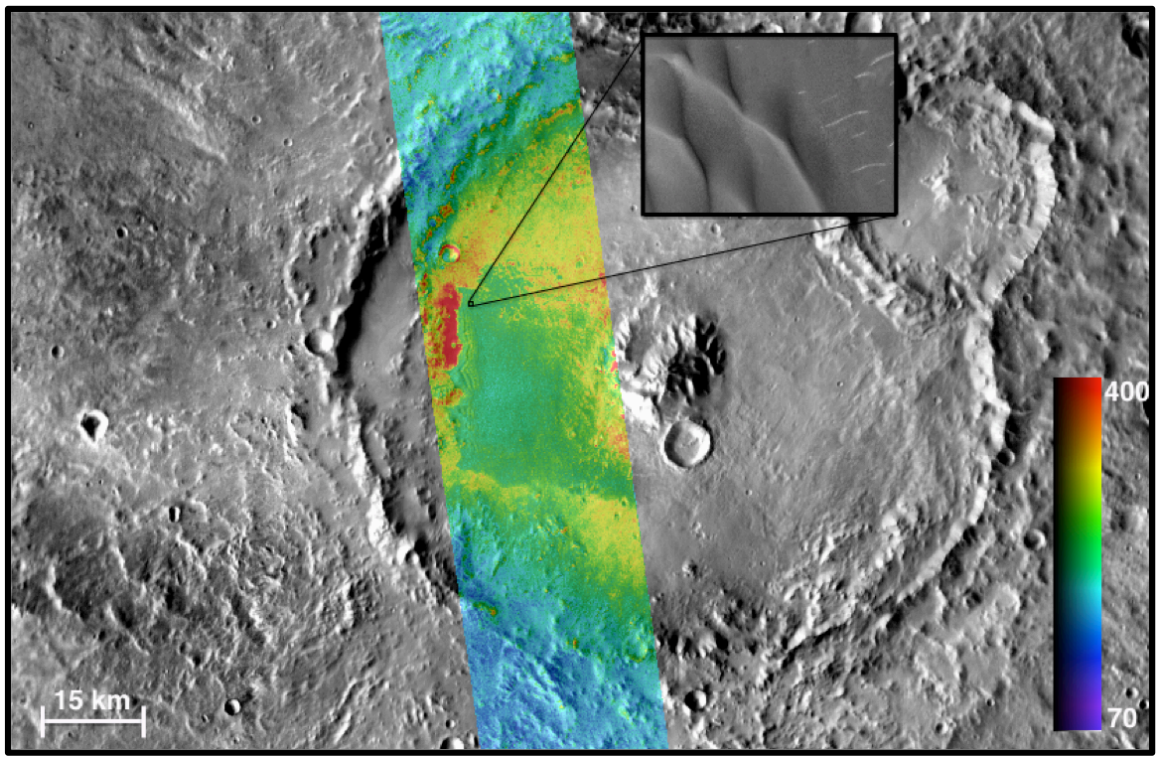

Figure 8. Schroeter crater dune field thermal inertia map derived from THEMIS IR nighttime observation I07869014 and superimposed on THEMIS daytime mosaic. Dune field sediment has a lower thermal inertia than the crater floor but a higher thermal inertia than the area surrounding the crater. Inset frame is a visible image (ESP_029894_1780) of a portion of the dune field from High Resolution Imaging Science Experiment (HiRISE) onboard Mars Reconnaissance Orbiter (MRO).

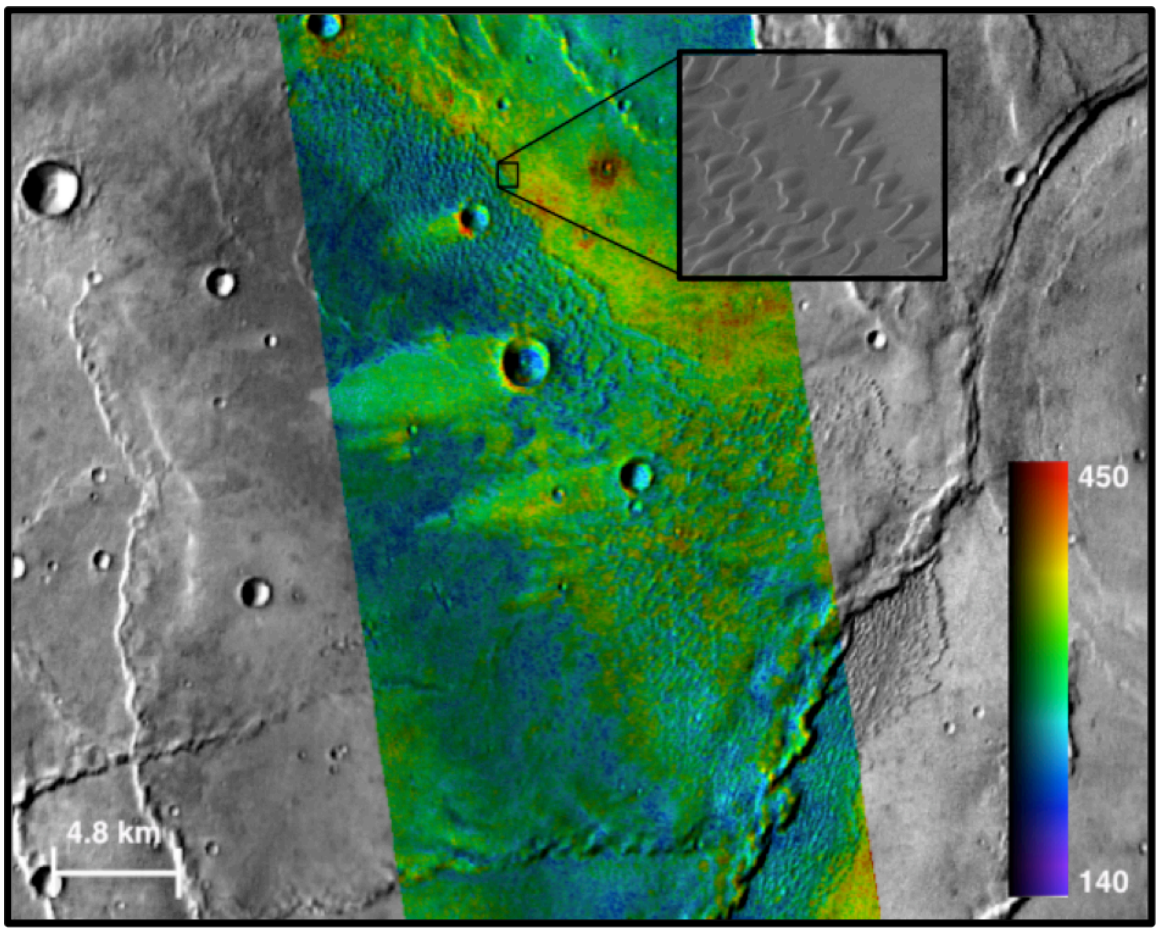

Figure 9. Meroe Patera dune field thermal inertia map derived from THEMIS IR nighttime observation I01602003 and superimposed on THEMIS daytime mosaic. Dune sediments generally had a lower thermal inertia (represented as shades of blue) than the surrounding areas. Inset frame is a visible HiRISE image (PSP_007754_1875) of barchanoid dunes. A portion of the Meroe Patera caldera is visible at far right.

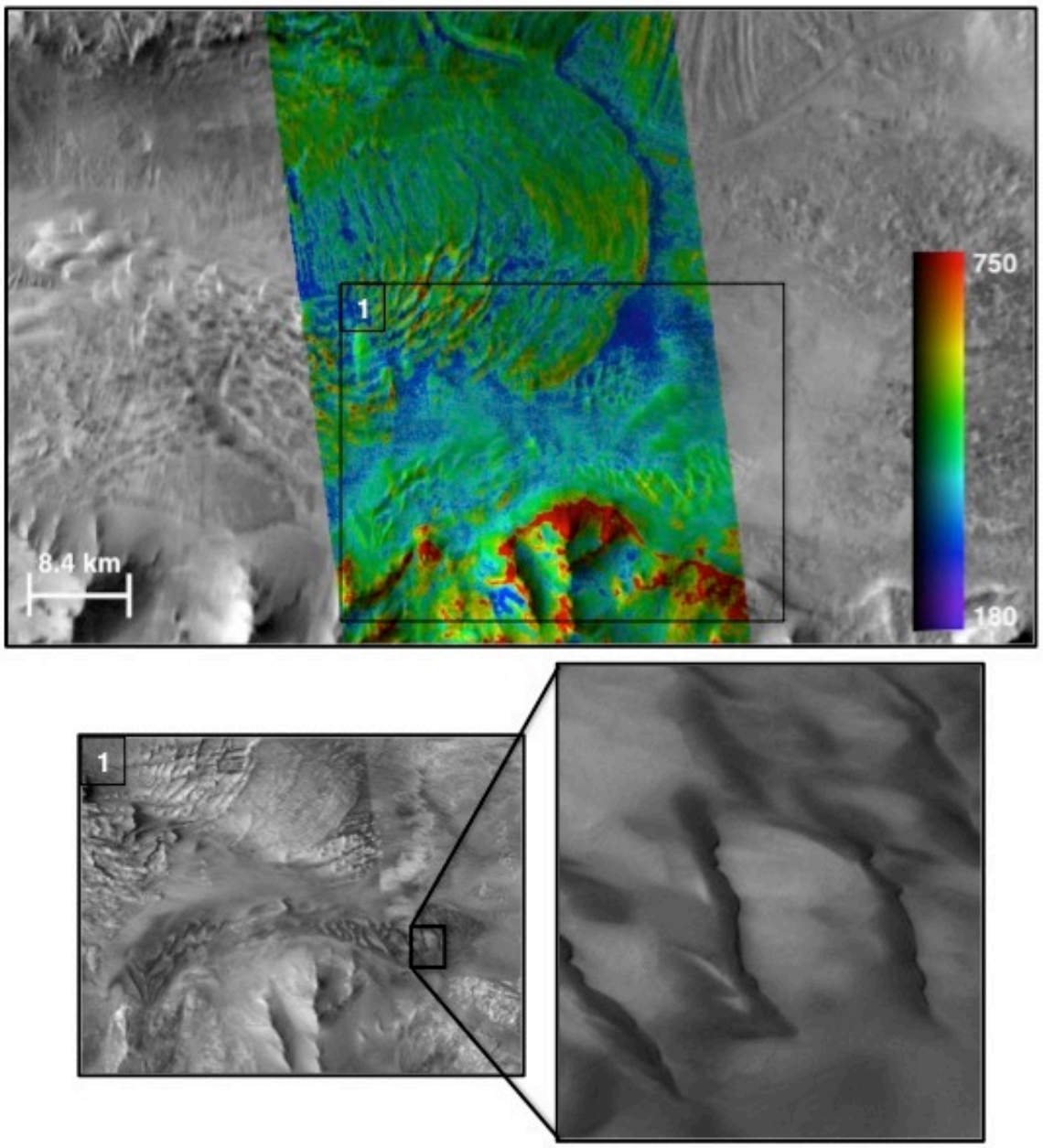

Figure 10. Valles Marineris dune field thermal inertia map derived from THEMIS IR nighttime observation I38709002 and superimposed on THEMIS daytime mosaic (top). The dune field contours the canyon wall with large landslide deposits to the north. Lower albedo (dark) sediments have elevated thermal inertia values, represented in shades of green while the higher albedo (light) sediments had lower thermal inertia values and are visible in shades of blue. Bottom left is two MRO Context Camera visible images (B09_013126_1707_XN_09S078W and B18_016739_1730_XN_07S077W) of the box outline from the thermal inertia map. HiRISE image (bottom right) shows the two sediment populations within the dune field (ESP_019218_1710).

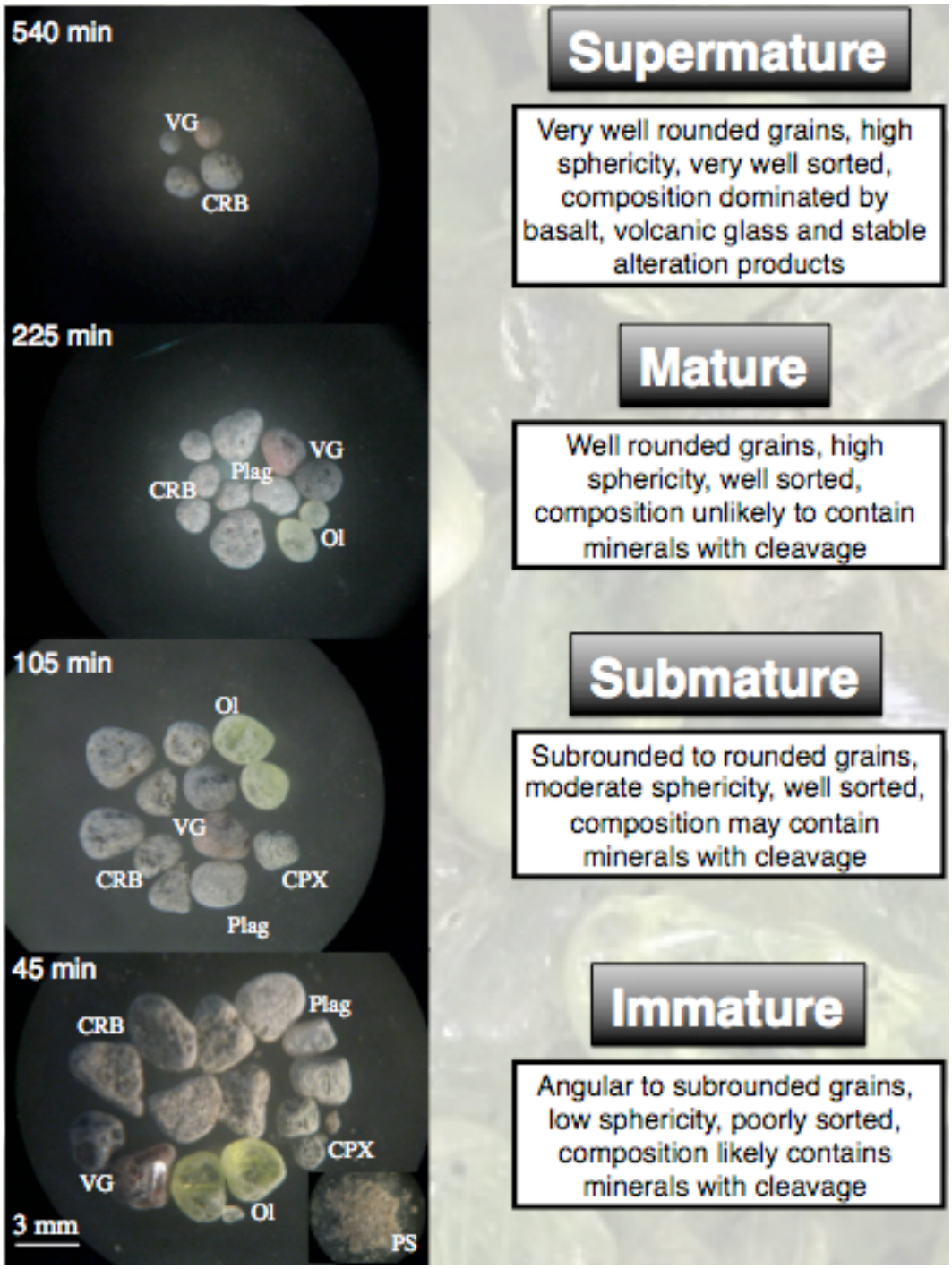

Figure 11. Results from heterogeneous sample abrasion at various time intervals. Bottom panel represents an example of a potential immature sediment composition and texture, while the top panel represents a super mature sediment. Minerals present include labradorite (plag), Columbia River Basalt (CRB), volcanic glass (VG), olivine (Ol), augite (CPX), and phyllosilicate (PS).